A&A 533, A83 (2011)
DOI: 10.1051/0004-6361/201117095

Astronomy & Astrophysics

SOPHIE velocimetry of *Kepler* transit candidates⋆

III. KOI-423b: an 18 $M_{\rm Jup}$ transiting companion around an F7IV star

F. Bouchy[1,2], A. S. Bonomo[3], A. Santerne[3], C. Moutou[3], M. Deleuil[3], R. F. Díaz[1,2], A. Eggenberger[4], D. Ehrenreich[4], C. Gry[1], T. Guillot[5], M. Havel[5], G. Hébrard[1,2], and S. Udry[6]

[1] Institut d'Astrophysique de Paris, UMR7095 CNRS, Université Pierre & Marie Curie, 98bis boulevard Arago, 75014 Paris, France
e-mail: bouchy@iap.fr
[2] Observatoire de Haute-Provence, Université d'Aix-Marseille & CNRS, 04670 Saint-Michel l'Observatoire, France
[3] Laboratoire d'Astrophysique de Marseille, Université Aix-Marseille, CNRS, 38 rue Frédéric Joliot-Curie, 13388 Marseille, France
[4] UJF-Grenoble 1/CNRS-INSU, Institut de Planétologie et d'Astrophysique de Grenoble, UMR 5274, 38041 Grenoble, France
[5] Université de Nice-Sophia Antipolis, CNRS UMR 6202, Observatoire de la Côte d'Azur, BP 4229, 06304 Nice Cedex 4, France
[6] Observatoire de Genève, Université de Genève, 51 Ch. des Maillettes, 1290 Sauverny, Switzerland

Received 17 April 2011 / Accepted 20 July 2011

ABSTRACT

We report the strategy and results of our radial velocity follow-up campaign with the SOPHIE spectrograph (1.93-m OHP) of four transiting planetary candidates discovered by the *Kepler* space mission. We discuss the selection of the candidates KOI-428, KOI-410, KOI-552, and KOI-423. KOI-428 was established as a hot Jupiter transiting the largest and the most evolved star discovered so far and is described by Santerne et al. (2011, A&A, 528, A63). KOI-410 does not present radial velocity change greater than 120 m s^{-1}, which allows us to exclude at 3σ a transiting companion heavier than 3.4 $M_{\rm Jup}$. KOI-552b appears to be a transiting low-mass star with a mass ratio of 0.15. KOI-423b is a new transiting companion in the overlapping region between massive planets and brown dwarfs. With a radius of 1.22 ± 0.11 $R_{\rm Jup}$ and a mass of 18.0 ± 0.92 $M_{\rm Jup}$, KOI-423b is orbiting an F7IV star with a period of 21.0874 ± 0.0002 days and an eccentricity of 0.12 ± 0.02. From the four selected *Kepler* candidates, at least three of them have a Jupiter-size transiting companion, but two of them are not in the mass domain of Jupiter-like planets. KOI-423b and KOI-522b are members of a growing population of known massive companions orbiting close to an F-type star. This population currently appears to be absent around G-type stars, possibly due to their rapid braking and the engulfment of their companions by tidal decay.

Key words. planetary systems – brown dwarfs – binaries: eclipsing – techniques: photometric – techniques: radial velocities – techniques: spectroscopic

1. Introduction

Launched in March 2009, *Kepler* is the second space mission designed to find transiting exoplanets by high-accuracy photometry. This mission has already demonstrated its strong capability of detecting transiting exoplanet candidates. Thanks to radial velocity (RV) follow-up or/and transit timing variation it has established and characterized up to eight new transiting planetary systems from the super-Earth regime – *Kepler*-10b (Batalha et al. 2011) – to the massive and bloated Jupiter regime – *Kepler*-5b (Koch et al. 2010). From the 156 000 stars continuously observed by *Kepler*, 706 exoplanets candidates were first identified and 306 of them were published by Borucki et al. (2011a) in February 2010. To establish the planetary nature of these candidates, to assess the fraction of false positives, and to characterize the true mass and density of new transiting planets, we started a large program of RV follow-up with the SOPHIE high-resolution spectrograph mounted on the 1.93-m telescope at the Observatoire de Haute-Provence Observatory (Bouchy et al. 2009; Perruchot et al. 2008).

We present here the strategy and results of our first campaign during third quarter 2010 on the four *Kepler* objects of interest KOI-428, KOI-423, KOI-552, and KOI-410. Our first target KOI-428 was revealed as a transiting hot Jupiter with a radius of 1.17 ± 0.04 $R_{\rm Jup}$ and a mass of 2.2 ± 0.4 $M_{\rm Jup}$ orbiting the largest and the most evolved star (2.13 $R_\odot$ and 1.48 $M_\odot$) discovered so far with a transiting exoplanet. This planet KOI-428b, which also corresponds to the first *Kepler* planet established from the public data, was described by Santerne et al. (2011a).

2. Selection of *Kepler* candidates

A first set of 306 *Kepler* exoplanet candidates was published by Borucki et al. (2011a). These candidates are faint stars ($14 \leq m_V \leq 16$) that are not included in the ground-based observation follow-up conducted by the *Kepler* team. They were identified from the first 33.5-day segment of the science operations (Q1) from May 13 to June 15, 2009 with a temporal sampling of 29.4 min.

From this list of candidates, we defined a selection using the following criteria. We first removed all targets fainter than magnitude 14.7, which is close to the magnitude limit of the SOPHIE spectrograph. One hundred fifteen candidates have a *Kepler* magnitude in the range 13.9–14.7. We then extracted candidates with an estimated radius greater than 0.8 $R_{\rm Jup}$. Almost all the known transiting planets with $R \geq 0.8$ $R_{\rm Jup}$ have a mass

⋆ Based on observations made with the 1.93-m telescope at the Observatoire de Haute-Provence (CNRS), France.

Table 1. *Kepler* candidates from Borucki et al. (2011a) selected for the SOPHIE follow-up.

Kepler object of interest	*Kepler* input catalog	RA	Dec	*Kepler* mag	R_p[a] [R_{Jup}]	Period [days]	T_{eff} [K]	SOPHIE follow-up status
KOI-410.01	KIC-5449777	19h28m59.53s	+40d41′45.8″	14.5	1.07	7.217	5968	planet or DEB
KOI-423.01	KIC-9478990	19h47m50.46s	+46d02′03.5″	14.3	0.94	21.087	5992	brown-dwarf
KOI-428.01	KIC-10418224	19h47m15.29s	+47d31′35.8″	14.6	1.04	6.873	6127	planet
KOI-552.01	KIC-5122112	19h49m35.58s	+40d13′45.1″	14.7	1.00	3.055	6018	low-mass star

Notes. [(a)] Estimated radius of the transiting candidates.

higher than 0.4 M_{Jup}. Lower masses are difficult if not impossible to detect with SOPHIE in this range of stellar magnitude (Santerne et al. 2011b). We removed the monotransit candidates (with an estimated period longer than 33.5 days). This led to a list of 11 candidates. The last step was to try to privilege massive hot-Jupiter and brown-dwarf candidates with the aims of better understanding this class of massive objects, of further exploring the link between massive planets and brown dwarfs and of deriving the main properties of their parent stars. As discussed in Bouchy et al. (2011), almost all transiting massive planets and brown dwarfs are found to orbit F-type stars as a consequence of rapid rotators, independent of their age (Nordstrom et al. 1997). We then selected the four hottest stars in our list for our first campaign with an estimated effective temperature greater than 5900 K. The characteristics of these four targets are listed in Table 1.

More recently, Borucki et al. (2011b) have published an update of the *Kepler* exoplanet candidates from the analysis from the analysis of the second quarter (Q2) data lasting 88.7 days from June 20 to September 16, 2009. We thus downloaded from the MAST database[1] these two first quarters of the publicly available Kepler data for our selected candidates. We then combined our RV observations to the analysis of the candidates' Kepler light curves.

3. SOPHIE observations

We performed the RV follow-up of the four candidates with the SOPHIE spectrograph (Bouchy et al. 2009; Perruchot et al. 2008) installed on the 1.93 m telescope in the Observatoire de Haute-Provence, France. SOPHIE is a cross-dispersed, high-resolution fiber-fed echelle spectrograph, stabilized in pressure and temperature and calibrated with a thorium-argon lamp. It is mainly dedicated to measure high-accuracy RVs on solar-type stars for exoplanets and asteroseismology studies. SOPHIE is one of the key facilities in the RV follow-up of *CoRoT* and SWASP-North transiting planetary candidates. Data reduction pipeline, observational strategy, and analysis tools were developed to optimize the follow-up of transiting candidates.

Observations were made with the SOPHIE high efficiency mode, with a spectral resolution of 39 000 at 550 nm, and the slow CCD read-out mode. The obj_AB observing mode was used, i.e., without acquisition of the simultaneous calibration lamp in order to monitor the background sky on the second fiber. The typical intrinsic stability of SOPHIE does not require using the simultaneous calibration, and the sky fiber is crucial for removing the scattered moonlight (Santerne et al. 2011b). SOPHIE spectra were reduced with the online pipeline. Radial velocities were obtained by computing the weighted cross-correlation function (CCF) of the spectra using a numerical spectral mask corresponding to a G2V star (Baranne et al. 1996; Pepe et al. 2002).

Observations were carried out from 2010 July 15 to 2010 September 13. A total of 28 measurements with 1-hour exposure times were done corresponding to an equivalent of about four nights spread over 24 different nights. Such flexibility in the schedule of the observations is crucial to properly cover orbital phases of transiting candidates.

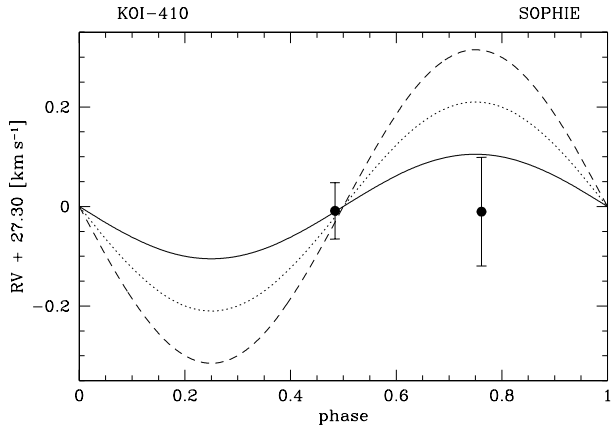

Fig. 1. Phase-folded SOPHIE radial velocity of KOI-410. The three curves correspond to the detection limit at 1, 2, and 3σ.

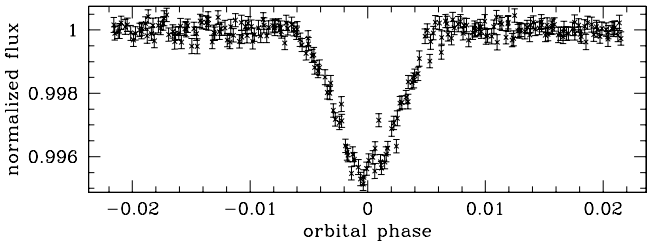

Fig. 2. Unbinned phase-folded transit light curve of KOI-410.

4. KOI-410

We made two SOPHIE measurements on this target. Phase-folded radial velocities are shown in Fig. 1 and present no significant variation at the level of 120 m s^{-1}. At 3-σ we can exclude a transiting companion with mass greater than 3.4 M_{Jup}. The transit light curve, shown in Fig. 2, is however, significantly V-shaped. The most probable contaminating star is KIC-5449780, which is an 18.4 *Kepler* magnitude star (36 times fainter) located at 9.6 arcsec. We estimated that, if this star was an eclipsing binary, it would cause a a displacement of the photocenter motion in the X and Y directions of more than 5 milli-pixels during the transit, a value excluded by the data (rms of

[1] http://archive.stsci.edu/kepler/data_search/search.php

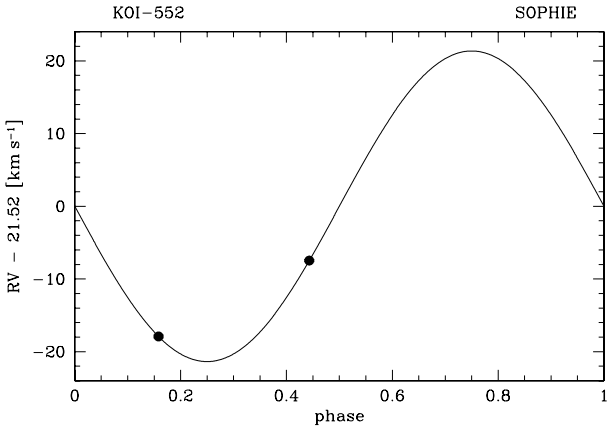

Fig. 3. Phase-folded SOPHIE radial velocity of KOI-552.

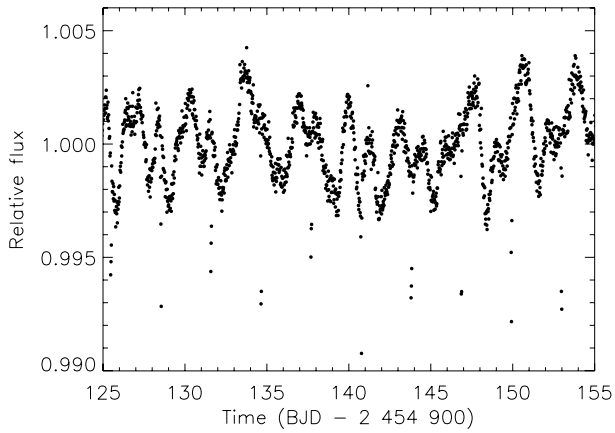

Fig. 4. A zoom of the KOI-552 light curve (Q2 data) showing flux variations due to starspots and, superposed, transits by a low-mass stellar companion.

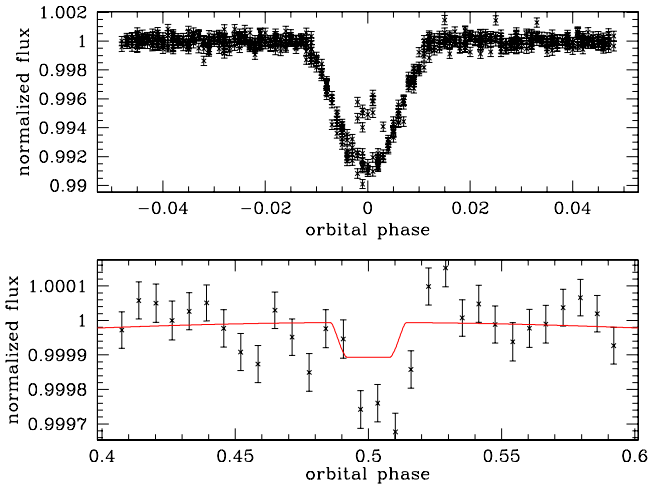

Fig. 5. Phase-folded light curve showing the unbinned primary transit (*upper panel*) and the binned secondary transit (*lower panel*) of KOI-552. The lower pannel also shows the expected model of the secondary transit for a hot Jupiter with a geometric Albedo of 1.

0.4 milli-pixel in both X and Y). This excludes the faint star located at 9.6 arcsec as the origin of the transit. We cannot exclude, however, an unresolved diluted eclipsing binary (DEB). To exclude a transiting giant planet with mass greater than 0.3 $M_{\rm Jup}$ at 3-σ requires additional RV measurements at the extrema phases with uncertainties of 10 m s^{-1}, which is beyond the capabilities of SOPHIE for such a faint star.

5. KOI-552

We made two SOPHIE measurements on this target (see Fig. 3). They show a large radial-velocity variation in phase with the *Kepler* ephemeris. Assuming a circular orbit – which is reasonable for a three-day period – the semi-amplitude K is 21.35 ± 0.14 km s^{-1} and reveals a low-mass transiting star with a mass ratio of 0.15.

The radius and mass for the central star are estimated to be 1.06 $R_\odot$ and 1.10 $M_\odot$ by Borucki et al. (2011b), respectively. The derived radius of the companion is then 1.0 $R_{\rm Jup}$. Such a radius seems small for an M-dwarf companion in this range of mass, where the typical radius is expected to be 0.17 $R_\odot$. Borucki et al. (2011b) recognize that some of the characteristics listed for the stars are uncertain, especially surface gravity. This might introduce errors in stellar diameters up to 25%. Our two SOPHIE spectra unfortunately have too low a signal-to-noise ratio (*S/N*) to determine the spectral type of KOI-552. From J & K magnitude and following the same procedure as for KOI-428b (Santerne et al. 2011a) and KOI-423b (see Sect. 6.2 in this paper), we estimate $T_{\rm eff}$ = 6560 ± 150 K assuming an [Fe/H] = −0.47 as provided in the KIC catalog, a value significantly higher than the estimation given by Borucki et al. (2011), $T_{\rm eff}$ = 6018 K. Assuming a solar metallicity changes the estimated $T_{\rm eff}$ within the uncertainties. If we assume that the effective temperature of the star is close to 6560 K, we may expect a larger stellar radius and thus a larger radius for the M-dwarf. We also note that the uncertainties on the impact parameter are large (b = 0.79 ± 0.24), because the transit is V-shape (see Fig. 5). An underestimation of the impact parameter could also explain the discrepancy in the M-dwarf radius. Our two SOPHIE spectra unfortunately have too low an *S/N* to determine the spectral type of KOI-552. Additional spectroscopy measurements are required to better characterize the parameters of the detected transiting companion.

From the MAST database, we downloaded the raw Kepler light curve containing photometric data from both the first and second quarters. We corrected the Q1 and Q2 light curves separately for long-term trends due to systematics and removed a few of the data points clearly affected by instrumental effects, such as those occurring just after the two safe mode events in the Q2 light curve (Haas et al. 2010; Jenkins et al. 2010). We estimated the flux excess due to stellar crowding in the Kepler mask by comparing the values of the median flux at the beginning of the raw Q1 and Q2 light curves with those of the corresponding error-corrected light curves (Jenkins et al. 2010). Finally, we subtracted the flux excess from each point of the Q1 and Q2 raw time series, separately. The treated light curve presents clear variations due to rotating stellar spots (see Fig. 4). The auto-correlation function of the light curve was computed after removing the transits, and a clear peak was found at $P_{\rm rot}$ = 3.08 ± 0.15 days indicating a possible spin-orbit synchronisation, which is expected for this mass ratio. The $v \sin i_\star$ derived from the CCF is estimated to 17.6 ± 1.0 km s^{-1}, which agrees with the measured rotational period and a stellar radius greater than 1 $R_\odot$. The transit light curve shown in Fig. 5 presents some transits that are shallower than others, which may be interpreted by the fact that the transiting companion crosses dark stellar spots. The stellar variability with a period equal or close to the orbital period prevents us from properly determining the

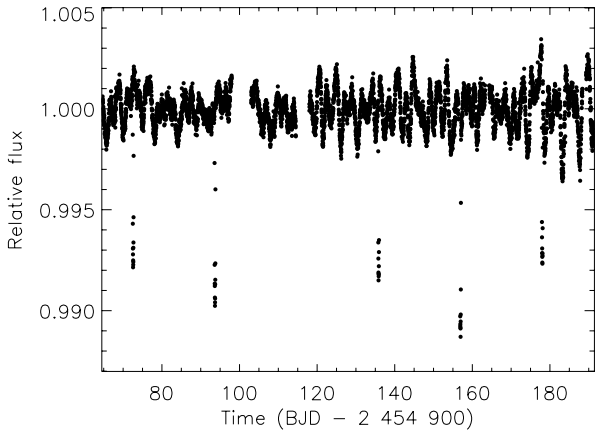

Fig. 6. The *Kepler* light curve of KOI423 with a temporal sampling of 29.4 min showing five transits and variations due to stellar activity.

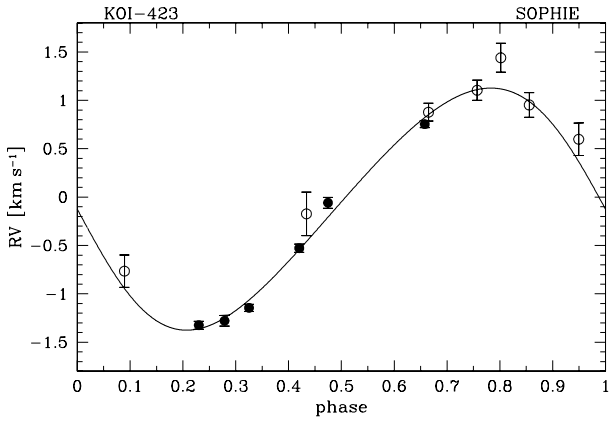

Fig. 7. Phase-folded radial velocity of KOI-423 with the best Keplerian orbit fit. Open dots correspond to measurements affected and corrected by the scattered moonlight.

ellipsoidal modulation and the beaming effect (van Kerkwijk et al. 2010).

The *Kepler* Q2 data, released on February 2011 after our spectroscopic observations, permit us to detect the secondary transit (see Fig. 5). The secondary transit is clearly too deep to be compatible with a perfect reflecting hot Jupiter with the orbital parameters of KOI-552 published in Borucki et al. (2011b). The occultation depth of ∼250 ppm would imply a geometric albedo of 2. Assuming a zero albedo, $T_{\rm eff}$ = 6560 K for the primary star, and radius ratio $R_{\rm c}/R_\star = 0.0967$, the effective temperature of the companion is estimated to be $T_{\rm eff}$ = 3300 K, which corresponds to an M 7 dwarf. Although we cannot exclude the possibility that a fraction of the observed depth might be due to reflected light, the secondary transit indicates a low-mass star companion.

The V-shape of the transit, the depth of the secondary eclipse, and the possible synchronisation between the companion and the star provide some evidence that this candidate was a very unlikely planetary candidate, although it was ranked as priority 2 by the *Kepler* team. Our two RV measurements definitively establish this candidate as a low-mass star.

6. KOI-423

6.1. Kepler light curve analysis

The target KOI-423 was observed by *Kepler* with a temporal sampling of 29.4 min for 122.2 days. The publicly-available *Kepler* light curve contains 5708 photometric measurements in total, after 135 data points were discarded by the *Kepler* pipeline as affected by systematic effects (Jenkins et al. 2010). The raw Q1 and Q2 light curves were downloaded from the MAST and treated in the same way as for KOI-552. The obtained Kepler light curve, shown in Fig. 6, exhibits five transits with a period of 21.1 days, a depth slightly shallower than 1% and a duration of about six hours. One additional transit should be observable but, unfortunately, it fell entirely inside a gap taking place from 2 455 014.5 to 2 455 016.7 (BJD). Furthermore, the fourth transit is only partially visible because of another data gap just before the ingress.

The KOI-423 light curve shows flux variations due to the presence of active regions on the photosphere, whose visibility is modulated by the stellar rotation. The peak-to-peak amplitude is ∼0.6%.

The standard deviation of the light curve, computed in a robust way after removing low frequency variations with a sliding median filter, is 2.5×10^{-4}, which is compatible with the median of the errors of the single photometric measurements, i.e. 2.1×10^{-4}.

To estimate the rotation period of the star, we computed the auto-correlation function of the *Kepler* light curve, after removing the five transits, and found a clear peak at $P_{\rm rot}$ = 4.35 ± 0.21 days. We also computed the Lomb-Scargle periodogram of the light curve (Scargle et al. 1982), and found power at 4.35, 2.17, and 1.45 days corresponding to the stellar rotation period and its two first harmonics.

Table 2. SOPHIE measurements of KOI-423.

BJD −2 455 000	RV [km s^{-1}]	$\sigma_{\rm RV}$ [km s^{-1}]	BIS [km s^{-1}]	*S/N*/pix @550nm
403.49308[a]	−0.173	0.225	–	8.2
425.43895	−0.059	0.056	−0.040	18.2
429.45136[a]	0.877	0.092	–	21.1
431.39644[a]	1.104	0.104	–	20.3
432.33993[a]	1.440	0.150	–	16.4
433.47474[a]	0.952	0.127	–	16.5
435.45034[a]	0.598	0.168	–	11.9
438.40205[a]	−0.765	0.167	–	11.0
441.36981	−1.324	0.041	0 −0.058	20.7
442.39937	−1.278	0.056	0 −0.088	18.4
443.37619	−1.145	0.037	0 −0.009	21.9
445.38001	−0.528	0.043	0 −0.198	22.7
450.39197	0.754	0.037	0 −0.145	23.5

Notes. [(a)] Measurements corrected from the scattered moonlight.

6.2. SOPHIE spectra and radial velocities

Thirteen measurements were made on this candidate with SOPHIE from 2010 July 26 to 2010 September 10. They are listed in Table 2. Seven of them were strongly affected by the scattered moonlight but corrected for radial velocity analysis using the sky spectra acquired simultaneously. In some exposures, the *S/N* on the sky fiber B, which points on the sky background, was even comparable to or greater than on the target fiber A, which is located on the target. We conservatively doubled the uncertainties of these seven measurements and did not use them to compute the bisector span.

The radial velocities shown in Fig. 7 present a clear variation in phase with the *Kepler* ephemeris and with a slight but significant eccentric orbit. The bisector span, listed in Table 2

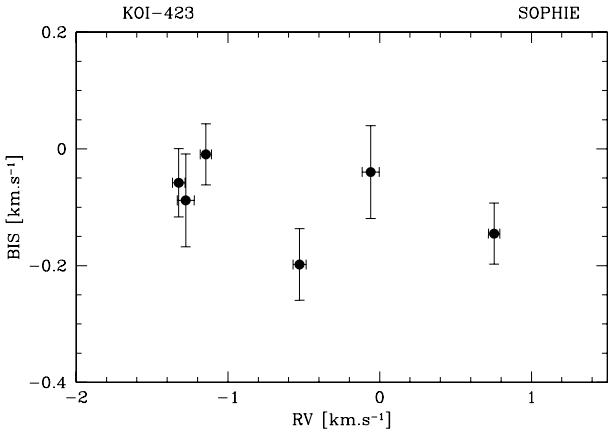

Fig. 8. Bisector span versus radial velocity of KOI-423 showing no correlation.

and shown in Fig. 8, does not reveal any significant variations at a level more than ten times smaller than the radial velocity variations allowing all scenarios of diluted and blended eclipsing binaries to be excluded.

We performed the spectroscopic analysis of the parent star using SOPHIE spectra. Individual spectra are too poor in quality to allow a proper spectral analysis. The six SOPHIE spectra not affected by the scattered moonlight were shifted to the barycentric rest frame and co-added order per order. We finally got a co-added spectrum with an *S/N* of about 110 per pixel on the continuum at 550 nm. From the analysis of a set of isolated lines, we derived a $v \sin i_\star$ of 16 ± 2.5 km s^{-1}. The spectroscopic analysis was carried out using the same methodology as for the *CoRoT* planets described in detail in Bruntt et al. (2010).

We limited the abundance analysis to the iron ions, because of the high $v \sin i_\star$ of the star and the quite moderate spectral resolution and *S/N* of the combined spectrum. In total 53 Fe I and 11 Fe II spectral lines were used for the temperature and $\log g$ determination. Following the Bruntt et al. (2008) methodology, abundances were measured differentially with respect to a SOPHIE solar spectrum. We found a marked underabundance of iron, with [Fe/H] = −0.29 ± 0.1. This result was further checked using the SOPHIE CCFs. Following the relations established by Boisse et al. (2010), we derived a $v \sin i_\star$ of 12.6 ± 1 km s^{-1} and an [Fe/H] of −0.18 ± 0.1 dex. The metallicity is 1-σ higher than the spectroscopic determination. The $v \sin i_\star$ value estimated from the CCF is 3-σ lower than then spectroscopic determination, which may come from the fact that the relation was calibrated assuming solar metallicity. The rotation velocity of KOI-423 derived from the stellar radius and the rotational period estimated from the light curve is 16.2 ± 1.7 km s^{-1}, in full agreement with the spectroscopic determination, indicating that $i_\star$ may be close to 90 deg.

The temperature derived from the Fe I – Fe II equilibrium is $T_{\rm eff}$ = 6260 ± 140 K. This is 2σ higher than the value of 5992 K quoted for the star in the Kepler Input Catalog. From infrared magnitudes J and K given in the 2MASS catalog, a reddening of $E(J-K)$ = 0.091 (from Cardelli et al. 1989), and Eq. (3) in Casagrande et al. (2010) assuming [Fe/H] = −0.3 dex, we derived an effective temperature $T_{\rm eff}$ = 6380 ± 150 K. This estimate agrees with our spectroscopic determination. As already mentioned for KOI-428 (Santerne et al. 2011a), the infrared determination of the effective temperature from Casagrande et al. (2010), based on stars of luminosity class IV and V, seems to be more reliable than the one used for the *Kepler* Input Catalog.

The surface gravity was estimated using pressure-sensitive lines: the Mg I 1b lines, the Na I D doublet, and the Ca I at 6122 and 6162 Å. As already noted by Bruntt et al. (2010), the results obtained on the Mg I triplet vary from one line to another due to the difficulty in the normalization of these broad lines. Fitting each of the observed lines of the triplet with synthetic spectra calculated using MARCS models, we found $\log g$ = 3.90 ± 0.25. The Na I D lines gave $\log g$ = 4.0 ± 0.2 and the Ca I lines $\log g$ = 4.1 ± 0.2. The latter are in good agreement with the value of $\log g$ = 4.2 obtained with VWA from the agreement between the Fe I and Fe II abundances. Considering the issue on the normalization for broad lines such as Mg I, we adopted as a final value the gravity derived from the Ca I pressure sensitive lines, that is, $\log g$ = 4.1 ± 0.20.

6.3. System parameters

System parameters were derived by performing the transit modeling and the Keplerian fit of the radial velocity measurements simultaneously. Transit fitting was carried out following the formalism of Gimenez (2006, 2009) after removing stellar variability in the out-of-transit light curve to correctly normalize the transits. For this purpose, we fitted a third-degree polynomial to the 9h intervals of the light curve before the ingress and after the egress of each transit. We discarded the fourth transit as only half visible, which prevented us from fitting the polynomial before the transit ingress and thus normalizing it as for the other ones.

The nine free parameters of our global best fit are the orbital period P, the transit epoch $T_{\rm tr}$, the transit duration $d_{\rm tr}$, the ratio of the companion to stellar radii $R_{\rm c}/R_\star$, the inclination i between the orbital plane and the plane of the sky, the Lagrangian orbital elements $h = e \sin\omega$ and $k = e \cos\omega$, where e is the eccentricity and ω the argument of the periastron, the radial-velocity semi-amplitude K, and the systemic velocity V_0. The two nonlinear limb-darkening coefficients $u_+ = u_a + u_b$ and $u_- = u_a - u_b$[2] were fixed in the transit modelling. They cannot be derived as free parameters because the transit ingress and egress are not sampled well, given the coarse temporal sampling of the *Kepler* light curves. The adopted limb-darkening coefficients u_a and u_b for the *Kepler* bandpass were taken from Sing's 2010 tables[3], after linearly interpolating at the $T_{\rm eff}$, $\log g$, and metallicity of the star: u_a = 0.303 ± 0.014 and u_b = 0.308 ± 0.005, which give u_+ = 0.611 ± 0.015 and u_- = −0.004 ± 0.015.

The best-fit parameters were found by using the algorithm AMOEBA (Press et al. 1992) and changing the initial values of the parameters with a Monte-Carlo method to find the global minimum of the χ^2. Following Kipping & Bakos (2011) and Santerne et al. (2011a), the transit modeling was performed with a temporal sampling five times denser than that of *Kepler*, i.e. one point every 5.88 min, and then binning the model samples to match the *Kepler* sampling rate. In such a way, the solution of the transit parameters is more accurate than a simple χ^2 minimization between the *Kepler* measurements and the transit model. Indeed, the *Kepler* sampling of 29.4 min inevitably smears all sharp changes occurring, such as transit ingress and egress (Kipping & Bakos 2011).

[2] u_a and u_b are the coefficients of the limb-darkening quadratic law: $I(\mu)/I(1) = 1 - u_a(1-\mu) - u_b(1-\mu)^2$, where $I(1)$ is the specific intensity at the center of the disk and $\mu = \cos\gamma$, with γ the angle between the surface normal and the line of sight.

[3] http://vega.lpl.arizona.edu/singd/David_Sing/Limb_Darkening.html

Table 3. KOI-423 system parameters.

Parameters	Value
Transit epoch $T_{\rm tr}$ [BJD]	$54972.5959^{+0.0006}_{-0.0005}$
Orbital period P [days]	21.0874 ± 0.0002
Transit duration T_{14} [h]	6.02 ± 0.09
Radius ratio $R_{\rm c}/R_\star$	$0.0896^{+0.0011}_{-0.0012}$
Inclination i [deg]	$88.83^{+0.59}_{-0.40}$
$h = e \sin\omega$	$0.120^{+0.022}_{-0.024}$
$k = e \cos\omega$	$-0.019^{+0.015}_{-0.012}$
Semi-amplitude K [km s^{-1}]	$1.251^{+0.030}_{-0.027}$
Systemic velocity V_0 [km s^{-1}]	$-0.101^{+0.017}_{-0.015}$
Orbital eccentricity e	$0.121^{+0.022}_{-0.023}$
Periastron argument ω [deg]	$98.9^{+5.9}_{-6.8}$
Scaled semi-major axis $a/R_\star$	$23.8^{+1.8}_{-1.7}$
$M_\star^{1/3}/R_\star$ [solar units]	$0.740^{+0.057}_{-0.051}$
Stellar density $\rho_\star$ [g cm^{-3}]	$0.57^{+0.14}_{-0.11}$
Impact parameter b	$0.43^{+0.11}_{-0.18}$
Effective temperature $T_{\rm eff}$[K]	6260 ± 140
Surface gravity $\log g$ [dex]	4.1 ± 0.2
Metallicity [Fe/H] [dex]	-0.29 ± 0.10
Rotational velocity $v \sin i_\star$ [km s^{-1}]	16 ± 2.5
Spectral type	F7IV
Star mass [$M_\odot$]	$1.10^{+0.07}_{-0.06}$
Star radius [$R_\odot$]	$1.39^{+0.11}_{-0.10}$
Distance of the system [pc]	1200 ± 250
Orbital semi-major axis a [AU]	0.155 ± 0.003
Companion mass $M_{\rm c}$ [$M_{\rm Jup}$]	$18.00^{+0.93}_{-0.91}$
Companion radius $R_{\rm c}$[$R_{\rm Jup}$]	$1.22^{+0.12}_{-0.10}$
Companion density $\rho_{\rm c}$ [g cm^{-3}]	$12.40^{+3.4}_{-2.6}$
Equilibrium temperature $T_{\rm eq}$ [K] [a]	905^{+39}_{-37}

Notes. [(a)] Black body equilibrium temperature for an isotropic planetary emission.

Fitted and derived system parameters are listed in Table 3, together with their 1-σ errors estimated using a bootstrap procedure. The last works as follows: 1) subtracts the best solution to the data; 2) shifts the photometric residuals, thus taking also possible correlated noise into account; 3) shuffles a fraction of the radial velocity residuals (typically $1/e \simeq 37\%$); 4) adds the subtracted solution; and 5) again carries out the global best fit. The limb-darkening parameters u_+ and u_- in the transit modeling were allowed to vary within their error bars related to the atmospheric parameter uncertainties. More than one thousand iterations were used for this procedure. Figure 7 shows the phase-folded radial velocity of KOI-423 with the best Keplerian fit. Figure 9 shows the phase-folded transit light curve of KOI-423 and, superposed, the transit model with a sampling rate of 5.88 min.

The star's mass and radius were estimated using a grid of STAREVOL evolutionary stellar tracks calculated for the *CoRoT* exoplanet program (Palacios, 2007, priv. com.). We used the regular approach for exoplanet host stars, which is the comparison of the star location in a ($T_{\rm eff}$, $M_\star^{1/3}/R_\star$) HR-plane to stellar

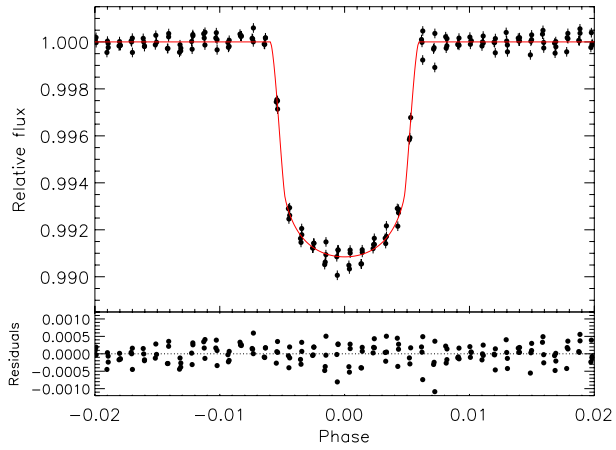

Fig. 9. *Top panel*: unbinned phase-folded *Kepler* transit light curve of KOI-423. The red solid line shows our oversampled transit model. *Bottom panel*: the residuals from the best-fit model.

evolutionary tracks with the appropriate range of metallicity. Using the $M_\star^{1/3}/R_\star$ from the transit modeling (see Table 3) and the effective temperature, we estimated the mass $M_\star = 1.10^{+0.07}_{-0.06}$ from the tracks and deduced the radius from this mass value and the $M_\star^{1/3}/R_\star$ values. Combining these mass and radius values we get $\log g = 4.20 \pm 0.2$, which is in good agreement with the spectroscopic value. With the adopted stellar parameters, we derived for the transiting companion $M_{\rm c} = 18.0 \pm 0.92\ M_{\rm Jup}$ and $R_{\rm c} = 1.22 \pm 0.11\ R_{\rm Jup}$.

The distance of the star can be estimated from the V magnitude ($m_v = 14.46$), a bolometric correction BC = −0.03 for F7IV stars (Straizys & Kuriliene 1981), the adapted solar bolometric magnitude ($M_{\rm bol,\odot} = 4.74$) recommended by Torres (2010), the reddening coefficient $A_V = 0.423$ provided by MAST database, and the stellar luminosity derived from the stellar radius and $T_{\rm eff}$. We find $d = 1200 \pm 250$ pc. The age was estimated to be 5.1 ± 1.5 Gyr and 4.4 ± 1.0 Gyr from the STAREVOL and the CESAM stellar evolution models, respectively. All the derived stellar parameters are reported in Table 3.

6.4. KOI-423b and the evolution of brown dwarfs and massive exoplanets

Figure 10 compares the size of KOI-423b to other known transiting objects from 5 $M_{\rm Jup}$ to the M-dwarf mass range. Its size is large, and it appears to be inflated, although comparable to other massive planets such as XO-3b (Johns-Krull et al. 2008). However, given its high mass, it lies farther from "classical" evolution tracks, such as those for isolated objects from Baraffe et al. (2003), than other known objects of this class. The problem is made even more acute when one considers that KOI-423b is relatively cold ($T_{\rm eq} = 905$ K), in contrast to most other objects in this plot, implying that irradiation effects cannot be held responsible for its anomalously large size.

In Fig. 11 we compare the constraints in age and radius obtained from photometric, spectroscopic, and CESAM stellar evolution models to dedicated evolution models including irradiation (see Guillot & Havel 2011; and Havel et al. 2011, for a description of the method). We first calculate a "standard" evolution track with a simplified semi-gray atmospheric boundary condition that has been parametrized to agree with radiative transfer calculations and evolution calculations (see Guillot 2010). Specifically, we adopt a thermal (infrared) opacity

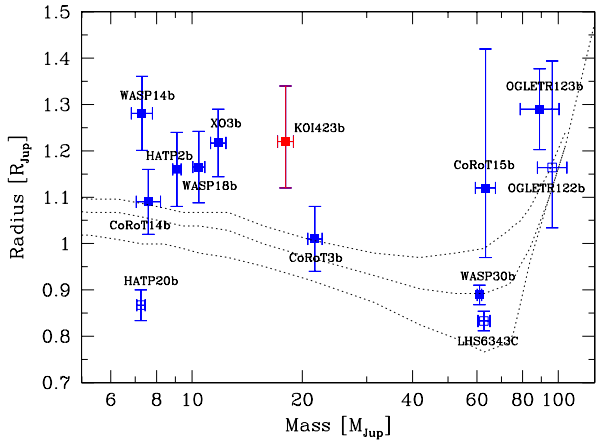

Fig. 10. Mass-radius diagram of massive transiting planets, eclipsing brown-dwarfs, and low-mass stars. Open symbols correspond to host stars with $T_{\rm eff} \leq 6000$ K. Dotted lines correspond to theoretical isochrones with ages 0.5, 1, and 5 Gyr (*from top to bottom*) from Baraffe et al. (2003).

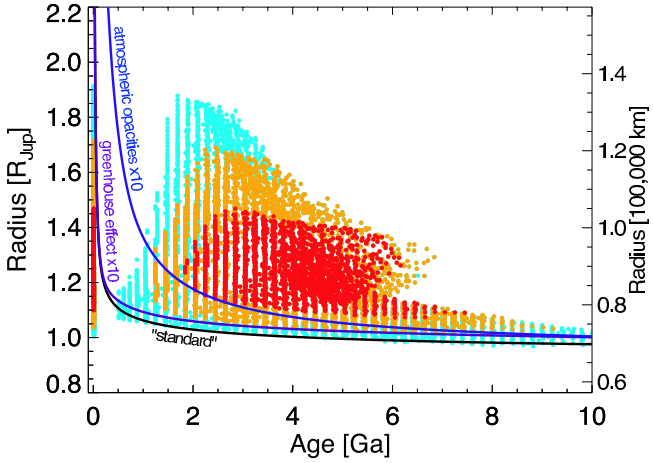

Fig. 11. Derived constraints on the radius of KOI-423b as a function of age compared to evolution models. The dots represent solutions within 1σ (red), 2σ (orange), and 3σ of the inferred $(T_{\rm eff}, \rho_\star)$ obtained from stellar evolution models. From bottom to top, the lines correspond to evolution calculations for a hydrogen-helium brown dwarf with $Y = 0.25$ using a "standard" evolution model (black line), a model in which the greenhouse factor has been arbitrarily multiplied by 10 (purple line), and a model in which the atmospheric opacities have been arbitrarily multiplied by 10 (blue line).

coefficient $\kappa_{\rm th} = 0.04$ cm^2 g^{-1} and a visible opacity $\kappa_{\rm v} = 0.024$ cm^2 g^{-1}. The corresponding evolution track is found to be at the 3σ lower limit of the main-sequence solutions. When we increase the greenhouse effect by a factor 10 by decreasing the visible opacity by the same factor, the consequence on the evolution is small. This is because the deep atmosphere is convective and weakly affected by a deeper penetration of the stellar light. Similarly, recipes commonly adopted to explain the large size of exoplanets of smaller sizes, including tides, dissipation of kinetic energy, or increased interior opacities (see Guillot 2008) have little effect on this very large planet. Even the possibility that only 50% of the atmosphere would be allowed to transfer heat efficiently (proposed by Bouchy et al. 2011, as one possibility to explain the large size of CoRoT-15b) does not work in this case. We also checked that the energy dissipation from the circularization of the orbit by tides is quite inefficient at the distance of KOI-423b. To obtain the required dissipation rates, one would need a tidal quality factor Q_p of about 10, i.e., at least 3 orders of magnitude over Jupiter's. In fact, the only way we found to reconcile models and observations within $\sim 1\sigma$ is to invoke an ad-hoc increase in the atmospheric opacities, by an order of magnitude or more (we used $\kappa_{\rm th} = 0.4$ cm^2 g^{-1} and $\kappa_{\rm v} = 0.24$ cm^2 g^{-1}). This is in essence similar to what is proposed by Burrows et al. (2007) for planets with lower masses. This yields a slower cooling of the object that remains large for a longer time.

However, the comparison between KOI-423b and CoRoT-3b (Deleuil et al. 2008) adds to the puzzle: the two companions have different sizes (CoRoT-3b lies where theory predicts it should be, KOI-423b is significantly larger), but they otherwise have very similar characteristics (mass, characteristics of the parent star). KOI-423 has $v \sin i = 16 \pm 2.5$ km s^{-1}, whereas CoRoT-3 has $v \sin i = 17 \pm 1$ km s^{-1}, showing that both are relatively fast rotators. CoRoT-3 has a metallicity close to the Sun ([M/H] $= -0.02 \pm 0.06$) when KOI-423b is metal-poor. The smallest massive planet HAT-P-20b (Bakos et al. 2010) orbits a host star with the strongest metallicity index [Fe/H] = 0.35. On one hand, this follows the trend observed at lower masses that planets around metal-rich stars contain more heavy elements and are therefore on average smaller (see Guillot 2008; Bouchy et al. 2010). On the other hand, one would expect that the atmosphere of KOI-423b is poorer in heavy elements, hence yielding smaller opacities, and potentially, a smaller size.

One natural possibility would be to invoke age as a way to distinguish between the two objects. However, given the estimated relatively high age, it is difficult to imagine that KOI-423 would be on the pre-main sequence (see Fig. 11), whereas CoRoT-3b would be much older. We cannot pretend that we understand the large radius of KOI-423.

6.5. Comparison to the population of massive exoplanets

For these systems with a known substellar companion, we plot in Fig. 12 the stellar effective temperature as a function of the companion mass for transiting objects or $M \sin i$ value for nontransiting objects. The data for low-mass companions (<13 $M_{\rm Jup}$) was obtained from exoplanets.org (see Wright et al. 2011) and exoplanet.eu. For objects with higher masses, no publicly available database exists, and we manually extracted parameters for the following transiting substellar systems: OGLE-TR-106 (Pont et al. 2005a), OGLE-TR-122 (Pont et al. 2005b), OGLE-TR-123 (Pont et al. 2005c), HAT-TR-205-013 (Beatty et al. 2007), CoRoT-15 (Bouchy et al. 2011), WASP-30 (Anderson et al. 2011), and LHS6343C (Johnson et al. 2011). And we did it for non-transiting short-period ($P < 30$ days) substellar systems: NLTT41135C (Irwin et al. 2010), HD 189310 (Sahlmann et al. 2011), and HD 180777 (Galland et al. 2006).

Although our ensemble of objects is clearly incomplete and derived from inhomogeneous databases, the lack of short period ($P < 10$ days), massive ($M_{\rm c} > 5\ M_{\rm Jup}$) companions around G-type stars ($T_{\rm eff}$ between 5000 and 6000 K) appears significant and puzzling. In comparison, these massive companions are routinely found next to F-type stars (including KOI-423). Given that selection biases would tend to favor their detection around G dwarfs, we believe that their absence is real.

The empty region is bounded very approximatively by the following objects: HAT-P-20b, a massive 7.5 $M_{\rm Jup}$, anomalously small (see Fig. 10) planet orbiting a K7 dwarf in 2.88 days; CoRoT-2b, an anomalously large 3.3 $M_{\rm Jup}$ planet orbiting a G7 dwarf in 1.74 days; CoRoT-14b, a 7.6 $M_{\rm Jup}$ planet orbiting an

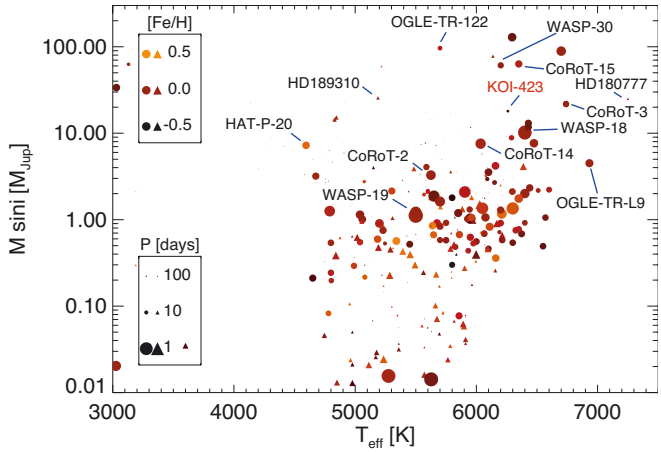

Fig. 12. Values of the stellar effective temperature and mass of the companion for systems containing a companion in the planet, brown dwarf, or M-dwarf mass range. Transiting/eclipsing systems are shown by circles, and systems only detected in radial velocimetry are shown by triangles (in which case the mass value corresponds to the mass times the sine of the inclination of the orbit with respect to the observer). The size (area) of the symbols is inversely proportional to the orbital period (see labels). The metallicity of the parent star is shown by the symbol color (see labels). Some objects deemed important for understanding the link between these parameters are labeled. The error bars on the masses are small (~10%) and would be barely visible in this diagram. The error bars on the effective temperatures are believed to range from ~100 K to up to ~300 K (for example for the faint OGLE-TR-122).

F9V star in 1.5 days; KOI-423b; WASP-30b, a 60 $M_{\rm Jup}$ brown-dwarf orbiting a relatively young (1−2 Ga) F8V star. At the top of the diagram, OGLE-TR-122b is a 96 $M_{\rm Jup}$ M dwarf on a 7.27-day orbit around an apparent G dwarf. However, in this case, given the faintness of the star and its poorly-determined $T_{\rm eff}$ (5700 ± 300 K), it may in fact also belong to the F-dwarf category.

Although this is not shown in Fig. 12, we believe that this trend continues well into the M-dwarf regime. For example, a study of 18 OGLE transit candidates with periods between 0.8 and 13.9 days (Bouchy et al. 2005) identified two planets (OGLE-TR-10b and OGLE-TR-56b; present in Fig. 12), 7 binaries consisting of an M-dwarf orbiting an F-dwarf and 1 M-dwarf around G-dwarf binary.

It is unlikely that massive companions do not form close to G-dwarfs or do not migrate there: the difference in mass between G-dwarfs and F-dwarfs (20%) is small compared to the extension in mass of the "G-dwarf companions desert" (from about 10 $M_{\rm Jup}$ to well within the stellar-mass regime). Following Bouchy et al (2011), we propose that close-in massive planets, brown dwarfs, or M-dwarfs may survive when orbiting orbiting close to F-dwarfs, but not when close to G-dwarfs. This could be because around G-dwarfs, the star would rapidly spin down and tidal interactions would lead to a migration and eventual engulfment of its companion. In contrast, around F-dwarfs, because of their small or absent convective zone, the much weaker braking (see e.g. Barker & Ogilvie 2009) will avoid the loss of angular momentum and the rapid decay of the companion's orbit.

Further work is required including both a proper statistical analysis of the observed correlations and models that combine the formation context, tidal, and magnetic interactions between the companions. Kepler will certainly help in providing a much more well-sampled comparison between F and G-dwarfs giant planetary companions.

7. Conclusions

The SOPHIE follow-up of four *Kepler* transiting candidates, selected with the aim of privileging massive planets and brown dwarfs, revealed at least three real massive transiting companions with Jupiter sizes: KOI-428b, a 2.2 $M_{\rm Jup}$ transiting planet (Santerne et al. 2011a); KOI-552b, a ~0.17 $M_{\odot}$ eclipsing low-mass star; and KOI-423b, a 18.0 $M_{\rm Jup}$ transiting companion. The status of the fourth candidate KOI-410 has not yet been solved, but we can exclude a companion heavier than 3.4 $M_{\rm Jup}$, and we still may suspect a possible background eclipsing binary. Our result shows that at least three *Kepler* candidates over the four selected are real Jupiter-size transiting objects, but only one of them, KOI-428b is in the mass domain of Jupiter-like planet.

KOI-423b is one of the rare types of transiting companions, like *CoRoT*-3b (Deleuil et al. 2008) that is located in the overlapping region between massive planet and brown dwarf and which may be considered either as a "superplanet" or a low-mass brown dwarf. As discussed in Sect. 6.4, its anomalous bloated radius is clearly not understood. Additional high *S/N* and high-resolution spectroscopic observations, as well as additional *Kepler* data, will permit us to better constrain the size of KOI-423b.

From RV surveys, only five massive planets or brown dwarfs ($M_{\rm c} \sin i > 5\ M_{\rm Jup}$) with short periods ($P < 30$ days) were found including HD 162020b (14.4 $M_{\rm Jup}$), HD 41004Bb (18.4 $M_{\rm Jup}$), HD 180777b (25 $M_{\rm Jup}$), HD 189310b (25.6 $M_{\rm Jup}$), and NLTT41135C (33.7 $M_{\rm Jup}$) respectively orbiting K2V, M2V, A9V, K2V, and M5V stars. Except for HD 180777b found in a dedicated RV surveys around A-F type star (Galland et al. 2006), this lack of short-period massive planets and brown dwarfs probably comes from the bias in the selection of RV surveys focusing on spectral types later than F5 and on slow rotators.

After our first SOPHIE campaign, Borucki et al. (2011b) published an update of the *Kepler* exoplanet candidates totalling 1235 candidates. Using the same criteria of selection as presented in Sect. 2 ($R \geq 0.8\ R_{\rm Jup}$, $m_v \leq 14.7$ and $T_{\rm eff} \geq 5900$ K), we found 17 additional candidates[4]. Radial velocity follow-up of these candidates may help to increase the statistic, and to further reveal the properties of massive planets and brown dwarfs, as well as to assess the true fraction of false positives in order to correctly interpret the *Kepler* candidate population.

Acknowledgements. We thank the technical team at the Observatoire de Haute-Provence for their support with the SOPHIE instrument and the 1.93-m telescope and, in particular, for the essential work of the night assistants. Financial support from the Programme national de planétologie (PNP) of the CNRS/INSU, France, and from the Swiss National Science Foundation (FNSRS) are gratefully acknowledged. We also acknowledge support from the French National Research Agency (ANR-08-JCJC-0102-01). A.S.B. is supported by a CNES grant. A.E. is supported by a fellowship for advanced researchers from the Swiss National Science Foundation.

References

Anderson, D. R., Collier Cameron, A., Hellier, C., et al. 2011, ApJ, 726, L19
Bakos, G. A., Hartman, J., Torres, G., et al. 2010, ApJ, submitted [arXiv:1008.3388]
Baraffe, I., Chabrier, G., Barman, T. S., et al. 2003, A&A, 402, 701
Baranne, A., Queloz, D., Mayor, M., et al. 1996, A&AS, 119, 373
Barker, A., & Ogilvie, G. I. 2009, in Cosmic Magnetic Fields: From Planets, to Stars and Galaxies, Proc. International Astronomical Union, IAU Symp., 259, 295
Batalha, N. M., Borucki, W. J., Bryson, S. T., et al. 2011, ApJ, 729, 27

[4] This list includes the recently announced Kepler-14b (Bucchave et al. 2011), a close-in massive planets of 8.4 $M_{\rm Jup}$ orbiting close to an F-type star.

Beatty, T. G., Fernandez, J. M., Latham, D. W., et al. 2007, ApJ, 663, 573
Boisse, I., Eggenberger, A., Santos, N. C., et al. 2010, A&A, 523, 88
Borucki, W. J., Koch, D. G., Basri, G., et al. 2011a, ApJ, 728, 117
Borucki, W. J., Koch, D. G., Basri, G., et al. 2011b, ApJ, 736, 19
Bouchy, F., Pont, F., Melo, C., et al. 2005, A&A, 431, 1105
Bouchy, F., Hébrard, G., Udry, S., et al. 2009, A&A, 505, 853
Bouchy, F., Hebb, L., & Skillen, I. 2010, A&A, 519, A98
Bouchy, F., Deleuil, M., Guillot, T., et al. 2011, A&A, 525, A68
Bruntt, H., De Cat, P., & Aerts, C. 2008, A&A, 478, 487
Bruntt, H., Deleuil, M., Fridlund, M., et al. 2010, A&A, 519, A51
Bucchave, L. A., Latham, D. W., Carter, J. A., et al. 2011, ApJ, submitted [arXiv:1106.5510]
Burrows, A., Hubeny, I., Budaj, J., & Hubbard, W. B. 2007, ApJ, 661, 502
Cardelli, J. A., Calyton, G. C., & Mathis, J. S. 1989, ApJ, 345, 245
Casagrande, L., Ramirez, I., Melendez, J., et al. 2010, A&A, 512, A54
Deleuil, M., Deeg, H., Alonso, R., et al. 2008, A&A, 491, 889
Ehrenreich, D., Lagrange, A. M., Bouchy, F., et al. 2011, A&A, 525, A85
Galland, F., Lagrange, A. M., Udry, S., et al. 2006, A&A, 452, 709
Giménez, A. 2006, A&A, 450, 1231
Giménez, A. 2009, in The Eighth Pacific Rim Conference on Stellar Astrophysics: A Tribute to Kam Ching Leung, ed. B. Soonthornthum, S. Komonjinda, K. S. Cheng, & K. C. Leung, ASP Conf Ser., 404, 291
Guillot, T. 2008, PhST, 130, 4023
Guillot, T. 2010, A&A, 520, A27
Guillot, T., & Havel, M. 2011, A&A, 527, A20
Haas, M., Batalha, N., Bryson, S., et al. 2010, ApJ, 713, 115
Havel, M., Guillot, T., Valencia, D., & Crida, A. 2011, A&A, 531, A3
Irwin, J., Buchhave, L., Berta, Z. K., et al. 2010, ApJ, 718, 1353
Jenkins, J. M., Caldwell, D. A., Chandrasekaran, H., et al. 2010, ApJ, 713, L120
Johnson, J. A., Apps, K., Gazak, J. Z., et al. 2011, ApJ, 730, 79
Johns-Krull, C., McCullogh, P., Burke, C., et al. 2008, ApJ, 677, 657
Kipping, D. M., & Bakos, G. A., 2011, ApJ, 733, 36
Koch, D. G., Borucki, W. J., Rowe, J. F., et al. 2010, ApJ, 713, 131
Nordstrom, B., Stefanik, R. P., Latham, D. W., et al. 1997, A&AS, 126, 21
Pepe, F., Mayor, M., Galland, F., et al. 2002, A&A, 388, 632
Perruchot, S., Kohler, D., Bouchy, F., et al. 2008, in Ground-based and Airborn Instrumentation for Astronomy II, ed. I. S. McLean, & M. M. Casali, Proc. SPIE, 7014, 70140J
Pont, F., Bouchy, F., Melo, C. M. F., et al. 2005a, A&A, 438, 1123
Pont, F., Melo, C. H. F., Bouchy, F., et al. 2005b, A&A, 433, L21
Pont, F., Moutou, Bouchy, F., et al. 2005c, A&A, 433, L21
Press, W. H., Teukolsky, S. A., Vetterling, W. T., & Flannery, B. P. 1992, Numerical recipes in FORTRAN, The art of scientific computing, 2nd edn. (Cambridge: University Press)
Sahlmann, J., Ségransan, D., Queloz, D., et al. 2011, A&A, 525, A95
Santerne, A., Diaz, R. F., Bouchy, F., et al. 2011a, A&A, 528, A63
Santerne, A., Endl, M., Hatzes, A., et al. 2011b, in Detection and Dynamics of Transiting Exoplanets, St. Michel l'Observatoire, France, ed. F. Bouchy, R. Diaz, & C. Moutou, EPJ Web Conf., 11, 02001
Scargle, J. D. 1982, ApJ, 263, 835
Sing, D. K. 2010, A&A, 510, A21
Straizys, V., & Kuriliene, G. 1981, Ap&SS, 80, 353
Torres, G. 2010, AJ, 140, 1158
Udry, S., Mayor, M., Naef, D., et al. 2002, A&A, 390, 267
van Kerkwijk, M. H., Rappaport, S. A., Breton, R. P., et al. 2010, ApJ, 715, 51
Wright, J. T., Fakhouri, O., Marcy, G. W., et al. 2011, PASP, 123, 412